Nuclear Instruments and Methods in Physics Research A 1068 (2024) 169763

Contents lists available at ScienceDirect

Nuclear Inst. and Methods in Physics Research, A

journal homepage: www.elsevier.com/locate/nima

The new and complete Belle II DEPFET pixel detector: Commissioning and previous operational experience

P. Ahlburg [a], L. Andricek [i], V. Babu [d,1], A. Baur [d], F. Becherer [d], F. Bernlochner [a], J. Bilk [b], T. Bilka [d], A. Bolz [d], L. Cao [d], R. Dhayal [j], J. Dingfelder [a], Z. Doležal [j], R. Farkas [a], A. Frey [c], K. Gadow [d], G. Giakoustidis [a], M. Graf-Schreiber [d], Z. Gruberova [j], Y. Han [d], M. Hoek [f], J. Kehl [d], M. Khan [a], C. Kiesling [h], P. Kodyš [j], C. Koffmane [i], M. Krein [b], W. Kühn [b], H. Krüger [a], P. Kvasnička [j], J.S. Lange [b], P. Leitl [h], Q. Liu [d,2], T. Lück [g], C. Mariñas [k], D. Meleshko [b], H.G. Moser [h], C. Niebuhr [d], J. Ninkovic [i], B. Paschen [a], D. Pitzl [d], M. Reif [h], S.P. Reiter [b], R. Richter [i], J. Schmitz [a,*,3], B. Schwenker [c], M. Schwickardi [c], C. Sfienti [f], J. Skorupa [h], B. Spruck [f], S. Stefkova [e], R. Stever [d], M. Takahashi [d], B. Wang [h], N. Wermes [a], R. Žlebčík [j], Belle-II DEPFET and PXD Collaboration

[a] University of Bonn, 53115 Bonn, Germany
[b] Justus-Liebig-Universität Gießen, 35392 Gießen, Germany
[c] II. Physikalisches Institut, Georg-August-Universität Göttingen, 37073 Göttingen, Germany
[d] Deutsches Elektronen–Synchrotron, 22607 Hamburg, Germany
[e] Karlsruhe Institute of Technology, Hermann-von-Helmholtz-Platz 1, 76344 Eggenstein-Leopoldshafen, Karlsruhe, Germany
[f] Johannes Gutenberg University Mainz, 55099 Mainz, Germany
[g] Ludwig Maximilians University, 80539 Munich, Germany
[h] Max Planck Institute for Physics, D-80805 Munich, Germany
[i] Halbleiterlabor der Max–Planck-Gesellschaft, Otto-Hahn-Ring 6, D-81739 Munich, Germany
[j] Faculty of Mathematics and Physics, Charles University, 121 16 Prague, Czech Republic
[k] IFIC (UVEG/CSIC), Edificio Institutos de Investigación Apartado de Correos 22085, E-46071 Valencia, Spain

ARTICLE INFO

Keywords:
Belle II
DEPFET
Pixel detector
Vertex detector

ABSTRACT

The Belle II experiment at the SuperKEKB collider in Tsukuba, Japan, has collected e^+e^- collision data between 2019 and 2022. After reaching a record-breaking instantaneous luminosity of $4.71\times10^{34}\,\mathrm{cm}^{-2}\,\mathrm{s}^{-1}$ and recording a dataset corresponding to $424\,\mathrm{fb}^{-1}$, it completed its first planned long shutdown phase in December 2023. Aside from upgrades of the collider and detector maintenance, the shutdown was used for the installation of the two-layer Pixel VerteX Detector (PXD). As the innermost sub-detector, multiple scattering effects need to be reduced. PXD utilizes the Depleted P-channel Field Effect Transistor (DEPFET) technology, allowing for a material budget of 0.21% X_0 per layer. Each of the tracker's 40 modules consists of an array of 250×768 pixels with a pitch ranging from 50 μm×55 μm for the inner to 85 μm×55 μm for the outer layer yielding high gain and high signal-to-noise ratio while retaining about 99% hit efficiency. This article discusses the experience of the 4-year operation of the previous single-layer PXD in harsh background conditions as well as commissioning and testing of the fully-populated PXD2 during Long Shutdown 1.

Contents

Abbreviations: Pixel VerteX Detector, PXD; Depleted P-channel Field Effect Transistor, DEPFET; Silicon Vertex Detector, SVD

* Corresponding author.
E-mail address: jannes.schmitz@uni-bonn.de (J. Schmitz).

[1] Now at IPHC F-67037 Strasbourg, France.
[2] Now at University of Hawaii, Honolulu, USA.
[3] Speaker.

https://doi.org/10.1016/j.nima.2024.169763
Received 15 February 2024; Received in revised form 10 April 2024; Accepted 18 August 2024
Available online 20 August 2024

1. Introduction

The Belle II experiment is located at the SuperKEKB accelerator at the High Energy Accelerator Research Organization (KEK) in Tsukuba, Japan. With beam energies of 7 GeV for the electron beam and 4 GeV for the positron beam the collider is operating at the center-of-mass energy of the $\Upsilon(4S)$ resonance ($10.58\,\mathrm{GeV}\,c^{-2}$) [1]. This resonance decays almost exclusively into a $B\bar{B}$ meson pair. Targeting an instantaneous luminosity of $6\times10^{35}\,\mathrm{cm}^{-2}\,\mathrm{s}^{-1}$ and a data set corresponding to $50\,\mathrm{ab}^{-1}$ within the next decade will allow unmatched precision in a wide range of flavor physics measurements [2].

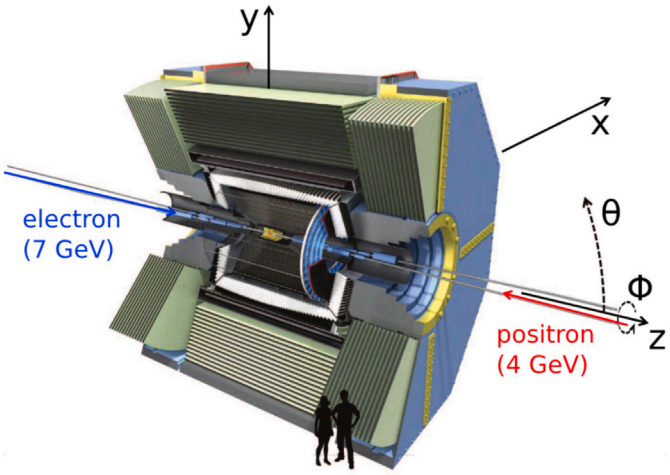

Fig. 1. 3D illustration of the Belle II detector cross-section including the Belle II coordinate system [3].

Fig. 1 shows a 3D illustration of the Belle II detector. It is an asymmetric multi-layer spectrometer covering almost 4π at the collision point. The outermost subsystem is the K_{Long}-Muon detector used for detection of muons and long-lived neutral kaons. Enveloping the inner sub-detectors, the superconducting solenoid coil provides a homogeneous magnetic field of 1.5 T along the beam axis z. The electromagnetic calorimeter uses CSI(Tl) scintillator crystals and encloses the detectors particle identification system. It is split up into two sub-detectors. The Time-of-Propagation counter covers the barrel region, while the Aerogel Ring Imaging Cherenkov detector is utilized to identify charged particles in the front-endcap region of the spectrometer. The Central Drift Chamber (CDC), a wire chamber, serves as the primary tracking device and surrounds the VerteX Detector (VXD) which provides high vertex resolution essential for measuring short flight paths and particle lifetimes. VXD itself is composed of a four-layer double-sided silicon strip detector (SVD) and the two-layer Pixel Vertex Detector (PXD) [4].

2. The Belle II Pixel Vertex Detector (PXD)

Based on the DEPFET (Depleted P-channel Field Effect Transistor) technology [5], PXD is the sub-detector closest to the Interaction Point (IP). It is the first full-scale detector to employ this technology in a High Energy Physics experiment.

2.1. DEPFET technology

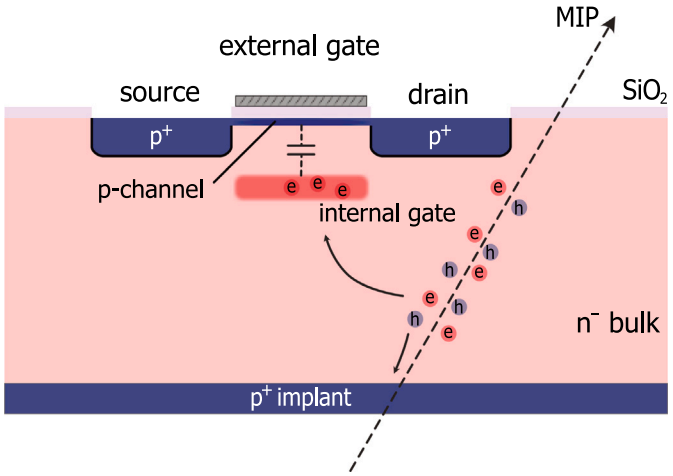

Fig. 2. Schematic cross-section of a DEPFET pixel cell [6].

Fig. 2 shows an illustration of the DEPFET pixel structure. A p-channel MOSFET is located on top of a fully depleted silicon n-bulk and is operated in saturation. An additional deep n-well, called the internal gate, is located underneath the transistor channel creating the potential minimum for electrons. To achieve bulk depletion, the p+ backside implantation is biased with high negative voltage of −50 V to −70 V through a punch-through contact on the front-side. Charged particles passing through the Si bulk will generate electron–hole pairs. The signal electrons produced by ionizing radiation drift into the internal gate with a charge collection time of a few nanoseconds, while the holes are removed from the volume after moving towards the p+ backside contact. To guide the drifting electrons to the internal gate, a p+ drift implantation surrounds the MOSFET structure. The accumulated charge in the internal gate modulates the source–drain current of the transistor, leading to an increase that constitutes the detection signal. The internal amplification g_q is derived from the change in source–drain current per unit charge, reaching values of up to 750 pA per electron located in the internal gate. To be prepared for the next readout cycle, all electrons must be removed from the internal gate after signal sampling. This clearing process is achieved by applying a high positive voltage pulse of 19 V to an additional n+ clear contact(see Table 1).

Table 1
Voltage configuration of the clear contact and DEPFET gate during the different operation phases. During charge collection, the respective pixels are turned off and signal charges can drift into the internal gate. By applying the negative gate voltage, the individual pixels can be turned on to read out the stable drain current in the sampling phase. Before returning to the charge collection phase, the internal gate is cleared via a positive voltage pulse on the clear contact. Typical operation voltage levels for an unirradiated module are $V_{clear} = [3\,V, 19\,V]$ and $V_{gate} = [-2.5\,V, 5\,V]$.

Phase	Clear voltage	Gate voltage	Duration
charge collection	low	high	≈20 µs
sampling	low	low	≈80 ns
clearing	high	low	≈25 ns

2.2. PXD modules

Fig. 3 shows a picture of a PXD sensor. Each so-called module is built in a self-supporting all-silicon design with a size of $(1.5 \times 8.5)\text{cm}^2$. It can be divided into three main regions.

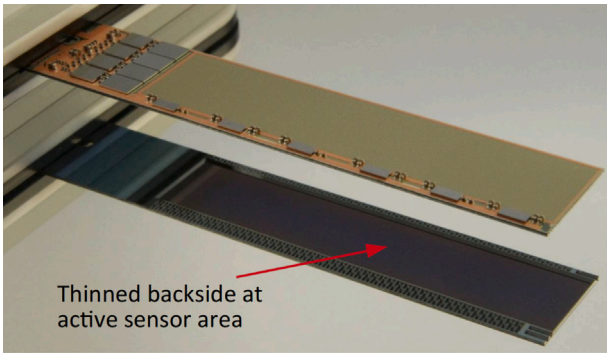

Fig. 3. Picture of a single PXD module. End-of-Stave and Balcony region are kept at a thickness of 450 µm to 525 µm, building the support frame and housing the different types of readout and steering ASICs. As highlighted with a red arrow in the mirror reflection of the backside, the active region is thinned down to 75 µm.

1. Active Area :
   The active sensor area consists of an array of 250 × 768 pixels with a pitch ranging from $(50 \times 55)\mu\text{m}^2$ for the inner to $(85 \times 55)\mu\text{m}^2$ for the outer layer.
2. Balcony :
   The balcony runs alongside the sensitive area and houses six Switcher Application-Specific Integrated Circuits (ASICs). They are responsible for the voltage switching of clear and gate voltages and therefore steer the rolling shutter readout of the module.
3. End-Of-Stave (EOS) :
   This is the region where eight readout ASICs are bump-bonded. The Drain Current Digitizers (DCDs) digitize the signals from the DEPFET pixels using 8-bit Analog-to-Digital Converters, resulting in good energy resolution. The Data Handling Processors (DHPs) are utilized for further processing of the digitized signal, including data reduction via zero suppression.

Combining the low noise of the design with the high internal amplification of the signal in the pixels results in an excellent Signal-to-Noise Ratio (SNR). As a result, the active area can be thinned downed to 75 µm while maintaining high particle detection efficiency. Additionally, achieving low material budget of only 0.21% X_0 per layer[4] minimizes the effects of multiple scattering.

[4] Mean value of one PXD ladder within the detector acceptance region ($17° < \Theta < 150°$). This includes the support balcony and all Switcher ASICs, but not the EOS region.

2.3. PXD detector design

To assemble the Belle II Pixel Detector four module types are necessary, depending on their position. Namely, forward, backward, inner layer and outer layer. A forward and a backward module are joined along the short edge of the sensor with a glue joint to form a so-called ladder. As seen in Table 2, the DCD and DHP ASICs are the main source of power consumption for a PXD module, requiring active cooling.

Table 2
Power consumption of a single PXD module, divided into components [7]. Most heat is produced by DCDs and DHPs at the EOS, requiring CO_2 cooling.

Device	Measured power
DCD	7.2 W
DHP	1.1 W
DEPFET sensor	0.2 W
Switcher	0.2 W
total	9 W

Therefore the EOS is mounted outside of the acceptance on the Support Cooling Block (SCB) and cooled by a two-phase CO_2 cooling system. Screw connection via an elongated hole allows for sensor gliding in case of thermal stress. Fig. 4 shows how a single PXD ladder is mounted on the support and cooling structure of a half-shell that is later directly mounted on the beampipe.

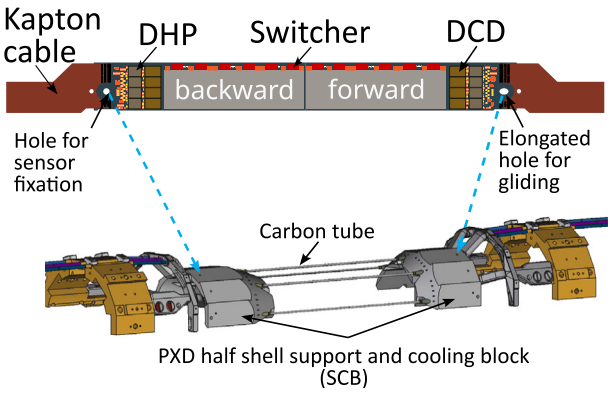

Fig. 4. 3D illustration of a PXD ladder and the PXD half-shell support and cooling block (SCB). Two PXD modules are glued to form a ladder and mounted on the support structure that features CO_2 cooling for the DCD and DHP regions, as well as outlets for N_2 cooling of pixel matrix and Switchers.

By sharing control signals among multiple pixels, the DEPFET pixel matrix is read out in a rolling shutter readout mode with four active matrix rows at once. Thus, the full matrix can be read out with approximately 20 µs integration time, while keeping the power consumption low. The heat produced by Switchers and the sensor matrix can be dissipated by cooled N_2 streaming from holes in the SCB and additional carbon tubes as seen in Fig. 4.

The two layers of PXD are mounted at radii of 14 mm and 22 mm as two half-shells in a windmill configuration, counting 8 ladders for the inner and 12 ladders for the outer layer.

3. PXD1 and previous operational experience

Due to delays in the gluing of outer ladders, only a partially populated pixel detector (PXD1) was installed for Run1 of the Belle II experiment. Two available outer ladders were used to cover the acceptance angle of a non-functional inner module. The ladder configuration that was used for the following results is depicted on the left-hand side in Fig. 5.

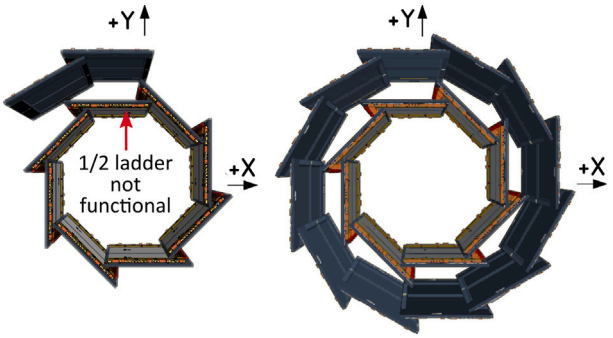

Fig. 5. Ladder configuration of PXD1 (left) and PXD2 (right). Due to setbacks in production PXD1 was installed with an incomplete configuration of the outer layer. Only two outer ladders were installed, covering a defective inner layer module. The fully populated PXD2 is shown on the right-hand side with the designed 40-module configuration.

3.1. Performance and efficiency

Multi-pixel clusters are generated by particles that traverse the pixel matrix at non-vertical angles, generating charge in multiple pixels. Considering the energy loss of charged particles in the detector and its energy resolution, the expected distribution is a sum of many Landau-Gaussian convoluted distributions. Over the course of three years detector operation, all PXD1 modules showed a homogeneous and stable most probable value (MPV) of the cluster charge distributions. By optimizing operation voltages in biweekly performance calibration scans, variations in track cluster charge could be kept below 10% over four years of operation. Fig. 6 shows the uniform distribution of cluster charge MPVs over an exemplary PXD1 module with ranges of 40 to 50 analog-to-digital-units (ADU). Where one ADU corresponds to ≈ 200 equivalent noise charges. With an excellent single pixel noise performance of <1 ADU, the signal to noise ratio was exceeding 50 ADU for some of the installed modules.

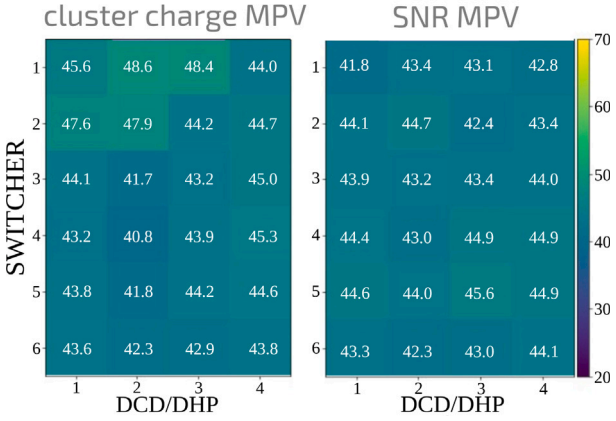

Fig. 6. PXD1 cluster charge and signal-to-noise MPV for a single module divided into ASIC regions. Over the operation timespan of 3 years signal and noise response remained homogeneous across the module matrices.

Furthermore, the PXD1 performance was examined using di-muon events with transverse momenta >2 GeV, studying the impact parameter resolution as a figure of merit. The resolution for the point of closest approach to the beam-spot in the z-direction was measured to be $\Delta z_0 = 20\,\mu\text{m}$ to $40\,\mu\text{m}$ depending on the dip angle of the muon track. For the x-y-plane a resolution of $\Delta d_0 = 10\,\mu\text{m}$ to $22\,\mu\text{m}$ was realized, depending on the azimuth angle of the muon track. Being in accordance to expectations from Monte-Carlo simulations, these numbers exceed the values recorded by the Belle experiment by a factor of 1.5 to 2. As a result of the improved impact parameter resolution, also the resolution for the D^0 lifetime measurement [8] was raised by a factor of ≈2 compared to BaBar and Belle experiments.

Another aspect to quantify PXD1 performance is the ratio of tracks with an associated cluster hit to the total number of tracks, given as hit efficiency. It can be determined by reconstructing CDC and SVD di-muon tracks and assigning PXD clusters [9]. Fig. 7 shows a rolled out hit efficiency map of PXD1 inner layer as a function of ϕ and z. In the functional active areas (fiducial region) the hit efficiency reached values of ≈99%. Over the period of Run1 PXD suffered from recurring sudden beam loss events within the accelerator. The high instantaneous radiation doses ($\mathcal{O}(1-10\,\text{Gy})$ within $40\,\mu\text{s}$) estimated for PXD1 might be explained by fireballs generated by the beam-induced fields leading to significant transverse kicks of beam bunches [10]. As a result, several single Switcher channels (steering 4 matrix rows each) or even a full Switcher were damaged by these beam losses. Inefficient Switcher channels are visible as thin white horizontal stripes in the efficiency map in Fig. 7. Taking also these dead and inactive regions into account (physics region), PXD1 hit efficiency remained at approximately 96% until the end of its operation.

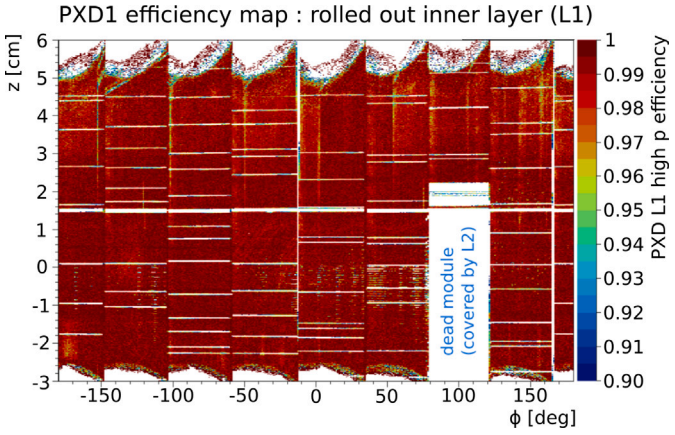

Fig. 7. PXD1 inner layer efficiency map as function of detector coordinates ϕ and z. In the rolled out representation single ladders are visible as vertical sections each separated by the glue gap around $z = 1.5\,\text{cm}$.

During dedicated measurement campaigns with a pulsed electron beam on PXD module components at the MAMI facility [11] the damage mechanism could be verified. It was shown that the voltage regulators within Switchers are susceptible to prompt irradiation bursts only if the module is fully powered [12]. Beside improvements in PXD power-down procedures during Long Shutdown 1, also additional sensors were implemented from accelerator side to further investigate and prevent hazardous beam conditions in the future.

3.2. Radiation dose and aging

Being designed for the end of Belle II lifetime, PXD modules and all its components are expected to be radiation tolerant up to approximately 200 kGy accumulated within 10 years of operation.

Fig. 8 shows an estimation of the integrated total ionizing dose of all inner forward modules during Run1. The evaluation is based on the sensors occupancy [13] and shows a non-uniform irradiation of modules depending on their position, originating from the beam crossing angles at the IP [14]. With 2.5 kGy the module surfacing the inner face of the accelerator ring (-x direction) received the lowest integrated dose. Module 1.1.1 in +x direction received the highest irradiation dose in accordance with the azimuthal dependency. While 6.5 kGy is still far from the expected lifetime exposure, irradiation induced detector aging required periodic readjustments.

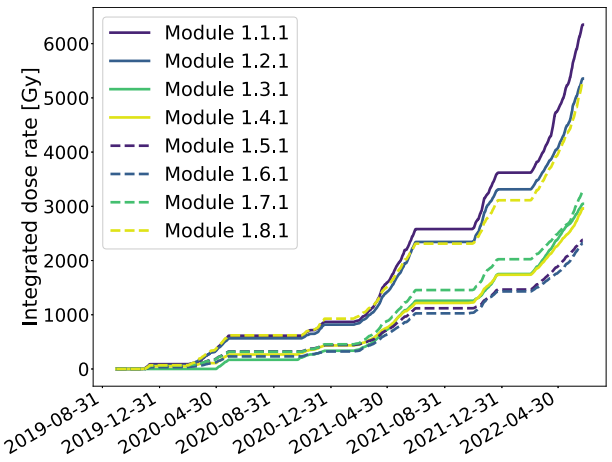

Fig. 8. Integrated dose of PXD1 first layer forward modules. The accumulated dose depends on the modules azimuthal position, peaking in $+x$ direction [13].

Main effect of radiation damage for PXD modules is trapping of oxide charges [15]. Fig. 9 shows the results of an Xray lab-campaign investigating the DEPFET gate voltage threshold shift with increasing total ionizing dose.

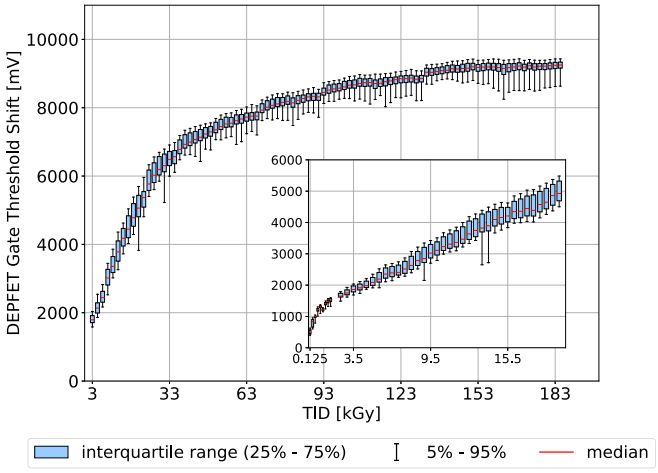

Fig. 9. Gate voltage threshold shift of irradiated PXD module in Xray lab campaign. The insert on the bottom right shows a cutout of the steep region in the lower dose region up to 20 kGy/.

The mechanism is well understood and gate voltages have been regularly adjusted to more negative values to keep the internal amplification constant.

4. PXD2 commissioning and first data

In a first pre-commissioning phase at DESY both PXD2 half-shells were individually tested utilizing a full-scale test setup. Along power supply system, CO_2 and nitrogen cooling and data read out chain, the test bench also contained a movable ^{90}Sr source enabling further calibration and characterization scans. After initial long-time operation of the first half-shell two inner ladders showed a noticeable kink at the glue joint. The cause of this incident could be traced back to the thermal expansion of the used aluminum dummy beam pipe along with non-optimal gliding functionality of the affected ladders. Damaged ladders were replaced and the half-shell was reconstructed incorporating minor changes to improve ladder gliding. After thorough investigations of the entire mechanical system also the screw torque for ladder fixation was reevaluated and reduced without significant loss of cooling efficiency. PXD2 was then shipped to KEK and mounted on the final titan/beryllium beam pipe in March 2023. In the last commissioning phase functionality of the full PXD2 system could be verified. Both SVD halves were installed around the PXD2 detector and inserted back into the Belle II detector after a combined commissioning phase in August 2023.

4.1. PXD2 expectations

Although the first layer of PXD has the highest impact on the performance of the reconstructed track impact parameters, PXD2 will widely benefit from the completed two-layer configuration. Expecting only a modest improvement in impact parameter resolution from the second layer, its main advantage will be an increased hit finding efficiency at higher background levels. The simulated data shown in Fig. 10 substantiates this enhancement for different background scenarios. Displaying the fraction of Monte-Carlo hits found in reconstructed tracks for a 1-layer PXD in the upper plot in direct comparison to a 2-layer PXD in the lower plot demonstrates the benefit especially for low transverse momentum particles at high detector occupancy. At occupancy levels of 2% and $p_t = 0.2$ GeV the expected increase in hit efficiency is around 20%.

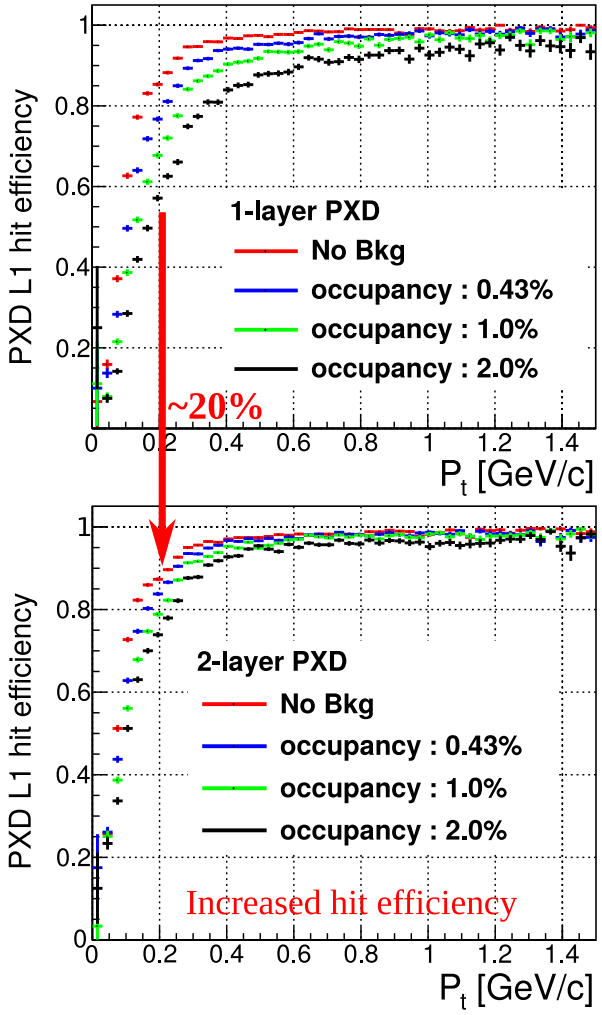

Fig. 10. PXD2 expected hit efficiency depending on transverse momentum and different occupancy scenarios obtained from MC simulations. PXD will mainly benefit from the completed two-layer configuration in high background scenarios with low p_t charged particles, increasing hit efficiency up to 20%.

4.2. First studies with cosmic particles

In September 2023 first cosmic particles were recorded for initial alignment and efficiency studies. To improve matching between PXD2 hits and SVD and CDC tracks, six rigid body alignment parameters and seven deformation parameters were determined for each VXD sensor. Fig. 11 shows first hit efficiency data for PXD2 taken without the solenoid's magnetic field by reconstructing SVD tracks. Inefficient regions originate from straight cosmic tracks passing through the gaps in the windmill structure. Since PXD is designed for the detection of curved tracks coming from the IP, these efficiency drops (e.g. $\phi \approx 30°$) are expected. Excluding low efficiency regions, which can be explained by the gaps between the two half-shells ($\phi \approx -15°$ and $\phi \approx 165°$) and four noisy modules needing further tuning (L1 $\phi \approx 135°$ or L2 $\phi \approx -30°$), a hit efficiency of $> 98\%$ was measured in large parts of the detector.

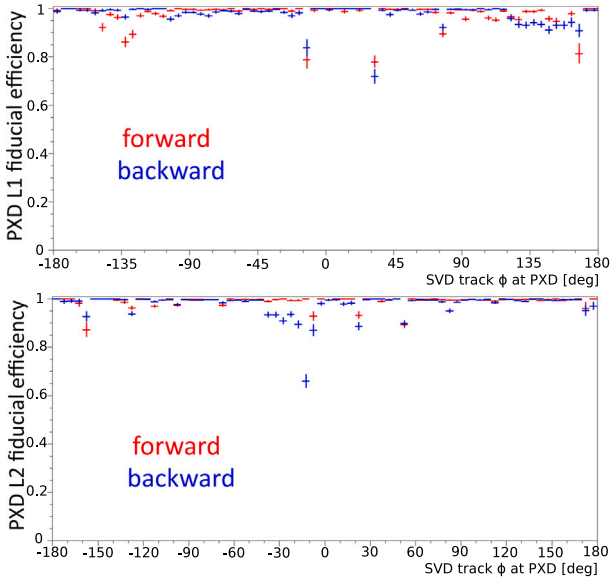

Fig. 11. First efficiency studies for PXD2 during cosmics data taking without magnetic field. (top) PXD2 inner layer hit efficiency and (bottom) outer layer hit efficiency. Since PXD is designed for curved tracks originating from the IP, straight cosmic tracks can traverse through gaps in the windmill structure. These gaps are visible as inefficient regions (e.g. $\phi \approx 30°$).

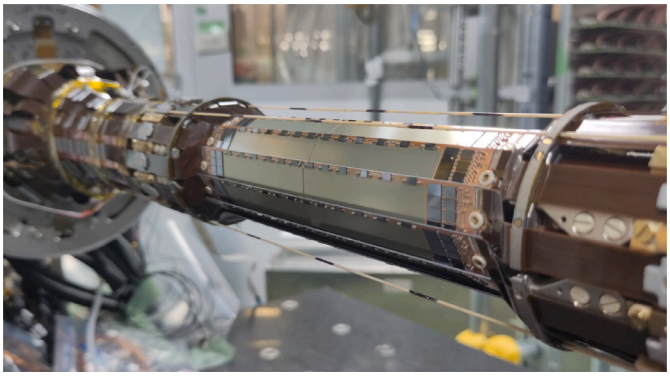

Fig. 12. PXD2 mounted on the titanium/beryllium beam pipe with active paraffin cooling. Before installing the new VXD into the Belle II detector, both SVD halves were installed around PXD2.

5. Summary and outlook

After four years of successful operation, the single layer PXD1 was replaced by the fully populated two-layer PXD2 in 2023 (see Fig. 12). PXD1 showed stable and homogeneous signal and noise response over all module matrices. The main operational challenges were sudden beam losses and the different beam backgrounds. While the overall efficiency of PXD1 remained at approximately 96% until the end of its operation, the experiment will benefit from the performance robustness of a two-layer configuration in high background conditions that are expected with increasing luminosity. Following various commissioning and testing phases in Germany and Japan, PXD2 was installed in the Belle II detector with 40 operable modules in August 2023. Excluding four modules which need further tuning, first studies with cosmic particles showed a hit efficiency exceeding 98% in most regions. The Belle II experiment is about to resume collision data taking mid of February 2024 with the new vertex detector configuration expected to operate at least until the next planned long shutdown at the end of this decade.

Declaration of competing interest

The authors declare that they have no known competing financial interests or personal relationships that could have appeared to influence the work reported in this paper.

References

[1] K. Akai, K. Furukawa, H. Koiso, SuperKEKB collider, Nucl. Instrum. Methods Phys. Res. A 907 (2018) 188–199.
[2] A. Natochii, et al., Measured and projected beam backgrounds in the Belle II experiment at the SuperKEKB collider, Nucl. Instrum. Methods Phys. Res. A 1055 (2023) 168550, http://dx.doi.org/10.1016/j.nima.2023.168550, URL https://www.sciencedirect.com/science/article/pii/S0168900223005405.
[3] T. Hara, T. Kuhr, Y. Ushiroda, Belle II Coordinate System and Guideline of Belle II Numbering Schem, 2011, Belle II Note, BELLE2-NOTE-TE-2015-009.
[4] T. Abe, et al., Belle II Technical Design Report, 2010, arXiv:1011.0352.
[5] J. Kemmer, G. Lutz, New detector concepts, Nucl. Instrum. Methods Phys. Res. A 253 (3) (1987) 365–377, http://dx.doi.org/10.1016/0168-9002(87)90518-3, URL https://www.sciencedirect.com/science/article/pii/0168900287905183.
[6] P. Ahlburg, Development of a Laboratory Readout System for DEPFET Pixel Detector Modules and Investigation of Radiation Backgrounds at the SuperKEKB Accelerator (Ph.D. thesis), Rheinische Friedrich-Wilhelms-Universität Bonn, 2023, URL https://hdl.handle.net/20.500.11811/10597.
[7] F. Müller, Characterization and optimization of the prototype DEPFET modules for the Belle II Pixel Vertex Detector (Ph.D. thesis), Ludwig-Maximilians-Universität München, 2017, URL http://nbn-resolving.de/urn:nbn:de:bvb:19-210714.
[8] F. Abudinén, et al., Belle II Collaboration Collaboration, Precise Measurement of the D^0 and D^+ Lifetimes at Belle II, Phys. Rev. Lett. 127 (2021) 211801, http://dx.doi.org/10.1103/PhysRevLett.127.211801, URL https://link.aps.org/doi/10.1103/PhysRevLett.127.211801.
[9] V. Bertacchi, et al., Track finding at Belle II, Comput. Phys. Comm. 259 (2021) 107610, http://dx.doi.org/10.1016/j.cpc.2020.107610, URL http://dx.doi.org/10.1016/j.cpc.2020.107610.
[10] T. Abe, High Energy Accelerator Research Organization (KEK) Collaboration, Fireball Hypothesis for the Trigger of Sudden Beam Losses at SuperKEKB, PASJ2023 127 (2023) 250, URL https://www-linac.kek.jp/mirror/www.pasj.jp/web_publish/pasj2023/proceedings/PDF/TUP0/TUP01.pdf.
[11] M. Dehn, K. Aulenbacher, F. Fichtner, P. Jennewein, W. Klag, H.-J. Kreidel, J. Röthgen, Pulsed operation at MAMI with high beam loading, in: 9th International Particle Accelerator Conference, 2018, http://dx.doi.org/10.18429/JACoW-IPAC2018-WEPAL023.
[12] J. Schmitz, Irradiation Burst Studies on Belle II PXD Module Components (Master thesis), University of Bonn, 2020.
[13] Y. Buch, Total Ionizing Dose Measurement of the Belle II Pixel Detector (Master thesis), Georg-August-University Göttingen, 2022.
[14] A. Moll, Comprehensive study of the background for the Pixel Vertex Detector at Belle II (Ph.D. thesis), Ludwig-Maximilians-Universität München, 2015, URL http://nbn-resolving.de/urn:nbn:de:bvb:19-191067.
[15] H. Schreeck, B. Paschen, P. Wieduwilt, P. Ahlburg, L. Andricek, J. Dingfelder, A. Frey, F. Lütticke, C. Marinas, R. Richter, B. Schwenker, Effects of gamma irradiation on DEPFET pixel sensors for the Belle II experiment, Nucl. Instrum. Methods Phys. Res. A 959 (2020) 163522, http://dx.doi.org/10.1016/j.nima.2020.163522, URL http://dx.doi.org/10.1016/j.nima.2020.163522.